



# Simulation of 3D Wave Propagation in Thermoelastic Anisotropic Media

José M. Carcione<sup>1,2</sup> · Enjiang Wang<sup>3</sup> · Ayman N. Qadrouh<sup>4</sup> · Mamdoh Alajmi<sup>4</sup> · Jing Ba<sup>3</sup>

Received: 15 March 2023 / Accepted: 6 March 2024  
© The Author(s), under exclusive licence to Springer Nature B.V. 2024

## Abstract

We develop a numerical algorithm for simulation of wave propagation in anisotropic thermoelastic media, established with a generalized Fourier law of heat conduction. The wavefield is computed by using a grid method based on the Fourier differential operator and a first-order explicit Crank-Nicolson algorithm to compute the spatial derivatives and discretize the time variable (time stepping), respectively. The model predicts four propagation modes, namely, a fast compressional or (elastic) P wave, a slow thermal P diffusion/wave (the T wave), having similar characteristics to the fast and slow P waves of poroelasticity, respectively, and two shear waves, one of them coupled to the P wave and therefore affected by the heat flow. The thermal mode is diffusive for low values of the thermal conductivity and wave-like (it behaves as a wave) for high values of this property. As in the isotropic case, three velocities define the wavefront of the fast P wave, i.e., the isothermal velocity in the uncoupled case, the adiabatic velocity at low frequencies, and a higher velocity at high frequencies. The heat (thermal) wave shows an anisotropic behavior if the thermal conductivity is anisotropic, but an elastic source does not induce anisotropy in this wave if the thermal properties are isotropic.

**Keywords** Thermoelasticity · Anisotropy · Thermal wave · Simulation · Fourier pseudospectral method

**Mathematics Subject Classification** 86-XX

## 1 Introduction

The theory of thermoelasticity combines heat conduction with elasticity. Specifically, it describes the coupling between the fields of deformation and temperature. Relevant geophys-

---

José M. Carcione is OGS Associate.

✉ J. Ba  
[jba@hhu.edu.cn](mailto:jba@hhu.edu.cn)

<sup>1</sup> School of Earth Sciences and Engineering, Hohai University, Nanjing, China

<sup>2</sup> National Institute of Oceanography and Applied Geophysics OGS, Trieste, Italy

<sup>3</sup> Key Lab of Submarine Geosciences and Prospecting Techniques, MOE, College of Marine Geosciences, Ocean University of China, Qingdao, 266100, China

<sup>4</sup> KACST, PO Box 6086, Riyadh 11442, Saudi Arabia

ical studies involve seismic attenuation (Zener [37]; Treitel [29]; Savage [23]; Armstrong [1]; Carcione [5]; Gurevich and Carcione [15]), geothermal exploration (e.g., Jacquey et al. [16]) and earthquake seismology (Boschi [4]). Basically, a heat source generates viscoelastic waves and a mechanical source induces a temperature field, whose flow equalizes the temperature difference with the surroundings giving rise to energy dissipation.

Biot [3], Deresiewicz [11], Savage [23] and Armstrong [1] used the Fourier law of heat conduction, but this formulation has unphysical solutions, and a more general system of equations has been proposed by Lord and Shulman [20] (with one relaxation time) and Green and Lindsay [14] (with two relaxation times) to overcome this problem. An alternative theory is presented by Sellitto et al. [24]. A plane-wave analysis for isotropic media has been performed by Rudgers [22], based on a relaxation term in the heat equation (Vernotte [30]; Cattaneo [10]) that converts the thermal diffusion to wave-like propagation with finite speeds at high frequencies. The theory predicts two P waves and an S wave, the latter not affected by the thermal effects (in homogeneous media). The P waves are an elastic wave (E wave) and a thermal wave (T wave) having similar characteristics to the fast and slow P waves of poroelasticity, respectively (Biot [3]). Carcione and co-workers solved the equations of isotropic thermoelasticity and thermo-poroelasticity with direct grid methods and, to our knowledge, simulated the T wave (2nd sound) and slow Biot wave (4th sound) jointly for the first time (Carcione et al. [6, 8, 9]; Wang et al. [35]). By grid method we mean a full-wave simulation algorithm, where the model is discretized on a mesh to which different properties can be assigned to the grid points.

The generalized theory of thermoelasticity developed by Lord and Shulman [20], extended to the anisotropic case, is essential when dealing with wave propagation in crystals, fibers and composites, and in general multilayered and fractured media. Tokuoka [28] considered plane waves, while Banerjee and Pao [2] performed a detailed plane-wave analysis, showing the four wavefronts present in thermoelastic-anisotropic media. Other authors who tackled the problem are Dhaliwal and Sherief [12], Kolyano and Shter [19], Sharma and Singh [26], Verma [31–33], Sharma [25] and Singh [27].

Phenomena such as negative thermal expansion (NTE) is a matter of study in several fields (e.g., photonics, electronics, medicine), where a combination of positive and negative linear thermal expansion coefficients is a consequence of high anisotropic elasticity. Romao et al. [21] found that thermal expansion anisotropy is correlated with elastic anisotropy: axes with negative thermal expansion are less compliant. Karunarathne et al. [18] analyzed a crystal, where temperature induces a negative Poisson ratio, a large linear negative thermal expansion, but positive Grüneisen parameters. A similar problem for layered media has been investigated by Wang et al. [36].

In this work, we solve the thermoelasticity equations for orthorhombic crystal symmetry equations by using the Fourier method to compute the spatial derivatives and an explicit time integration technique (e.g., Carcione [5, 9]). A plane-wave analysis, which provides the wavefronts and dissipation factors as a function of frequency and propagation direction, verifies the results, computed as snapshots of the wavefield. The computed wavefields, which cannot be obtained by an analytical method, (also for homogeneous media), constitute the novelty of this research. Moreover, the algorithm, being a direct modeling technique, allows us to handle spatially inhomogeneous media, as shown by the last example. Possible applications can be the computation of synthetic seismograms and wavefields for non-isothermal media, where the effect of temperature is important.

## 2 Equations of Thermoelasticity

Let us define by  $(x, y, z)$  the position vector,  $t$  the time variable,  $v_i$ ,  $i = 1, 2, 3$  the components of the particle velocity field, by  $\sigma_{ij}$  the components of the stress tensor and by  $T$  the increment of temperature above a reference absolute temperature  $T_0$  for the state of zero stress and strain. In orthorhombic media, the stress-strain relations of thermoelasticity are given by (Banerjee and Pao [2]; Verma [31–33]):

### 2.1 Rate of Strain-Particle Velocity Relations:

$$\begin{aligned}\epsilon_1 &= v_{x,x}, & \epsilon_2 &= v_{y,y}, & \epsilon_3 &= v_{z,z}, \\ 2\epsilon_{xy} &= v_{y,x} + v_{x,y}, \\ 2\epsilon_{xz} &= v_{z,x} + v_{x,z}, \\ 2\epsilon_{yz} &= v_{z,y} + v_{y,z},\end{aligned}\tag{1}$$

where  $\epsilon_{ij}$  denote the rate of strain components and the comma notation is used for spatial derivatives.

### 2.2 Stress-Strain Relations:

$$\begin{aligned}\dot{\sigma}_{xx} &= c_{11}\epsilon_1 + c_{12}\epsilon_2 + c_{13}\epsilon_3 - \beta_1\dot{T} - f_{xx}, \\ \dot{\sigma}_{yy} &= c_{12}\epsilon_1 + c_{22}\epsilon_2 + c_{23}\epsilon_3 - \beta_2\dot{T} - f_{yy}, \\ \dot{\sigma}_{zz} &= c_{13}\epsilon_1 + c_{23}\epsilon_2 + c_{33}\epsilon_3 - \beta_3\dot{T} - f_{zz}, \\ \dot{\sigma}_{xy} &= 2c_{66}\epsilon_{xy} - f_{xy}, \\ \dot{\sigma}_{xz} &= 2c_{55}\epsilon_{xz} - f_{xz}, \\ \dot{\sigma}_{yz} &= 2c_{44}\epsilon_{yz} - f_{yz},\end{aligned}\tag{2}$$

where  $c_{IJ}$  are the elastic constants, an overdot denotes time differentiation,

$$\begin{aligned}\beta_1 &= c_{11}\alpha_1 + c_{12}\alpha_2 + c_{13}\alpha_3, \\ \beta_2 &= c_{12}\alpha_1 + c_{22}\alpha_2 + c_{23}\alpha_3, \\ \beta_3 &= c_{13}\alpha_1 + c_{23}\alpha_2 + c_{33}\alpha_3,\end{aligned}\tag{3}$$

with  $\alpha_i$  the coefficients of thermal expansion and  $f_{ij}$  are external stress forces.

### 2.3 Equations of Momentum Conservation:

$$\begin{aligned}\partial_x\sigma_{xx} + \partial_y\sigma_{xy} + \partial_z\sigma_{xz} &= \rho\dot{v}_x + f_x, \\ \partial_x\sigma_{xy} + \partial_y\sigma_{yy} + \partial_z\sigma_{yz} &= \rho\dot{v}_y + f_y, \\ \partial_x\sigma_{xz} + \partial_y\sigma_{yz} + \partial_z\sigma_{zz} &= \rho\dot{v}_z + f_z,\end{aligned}\tag{4}$$

where  $\rho$  is the mass density and  $f_i$  are the components of external body forces.

### 2.4 Law of Heat Conduction:

$$\Delta_\gamma T = C(\dot{T} + \tau \ddot{T}) + T_0[\beta_1(\epsilon_1 + \tau \dot{\epsilon}_1) + \beta_2(\epsilon_2 + \tau \dot{\epsilon}_2) + \beta_3(\epsilon_3 + \tau \dot{\epsilon}_3)] + q, \quad (5)$$

with

$$\Delta_\gamma = (\gamma_1 T_{,x})_{,x} + (\gamma_2 T_{,y})_{,y} + (\gamma_3 T_{,z})_{,z}, \quad (6)$$

where  $\gamma_i$  are the coefficients of heat conduction (or thermal conductivity),  $C$  is the specific heat of the unit volume in the absence of deformation,  $\tau$  is a relaxation time, and  $q$  is a heat source. Equation (5) generalizes Eq. (2) of Verma [33] to the heterogeneous case, suitable for direct grid modeling.

Equations (1)-(6) yields the thermoelasticity equations of Carcione et al. [9] in the isotropic case, where

$$c_{11} = c_{22} = c_{33} = \lambda + 2\mu,$$

$$c_{12} = c_{13} = c_{23} = \lambda,$$

$$c_{44} = c_{55} = c_{66} = \mu,$$

$$\alpha_1 = \alpha_2 = \alpha_3 = \alpha,$$

$$\beta_1 = \beta_2 = \beta_3 = \beta,$$

and

$$\gamma_1 = \gamma_2 = \gamma_3 = \gamma,$$

where  $\lambda$  and  $\mu$  are the Lamé constants.

### 3 Differential Equations of Motion and Algorithm

We consider the 3D case and solve the differential equations by using the first-order time derivative approach, termed particle velocity-stress formulation in elasticity. Here, it is called particle velocity-stress-temperature formulation:

$$\dot{v}_x = \rho^{-1}(\partial_x \sigma_{xx} + \partial_y \sigma_{xy} + \partial_z \sigma_{xz} - f_x) = \Pi_x,$$

$$\dot{v}_y = \rho^{-1}(\partial_x \sigma_{xy} + \partial_y \sigma_{yy} + \partial_z \sigma_{yz} - f_y) = \Pi_y,$$

$$\dot{v}_z = \rho^{-1}(\partial_x \sigma_{xz} + \partial_y \sigma_{yz} + \partial_z \sigma_{zz} - f_z) = \Pi_z,$$

$$\epsilon_1 = \partial_x v_x, \quad \epsilon_2 = \partial_y v_y, \quad \epsilon_3 = \partial_z v_z,$$

$$\dot{\epsilon}_1 = \partial_x \Pi_x, \quad \dot{\epsilon}_2 = \partial_y \Pi_y, \quad \dot{\epsilon}_3 = \partial_z \Pi_z,$$

$$\dot{T} = \psi,$$

$$\dot{\psi} = (C\tau)^{-1} \{ \Delta_\gamma T - T_0[\beta_1(\epsilon_1 + \tau \dot{\epsilon}_1) + \beta_2(\epsilon_2 + \tau \dot{\epsilon}_2) + \beta_3(\epsilon_3 + \tau \dot{\epsilon}_3)] - q - C\psi \}, \quad (7)$$

$$\dot{\sigma}_{xx} = c_{11}\epsilon_1 + c_{12}\epsilon_2 + c_{13}\epsilon_3 - \beta_1\psi - f_{xx},$$

$$\dot{\sigma}_{yy} = c_{12}\epsilon_1 + c_{22}\epsilon_2 + c_{23}\epsilon_3 - \beta_2\psi - f_{yy},$$

$$\dot{\sigma}_{zz} = c_{13}\epsilon_1 + c_{23}\epsilon_2 + c_{33}\epsilon_3 - \beta_3\psi - f_{zz},$$

$$\dot{\sigma}_{xy} = c_{66}(\partial_x v_y + \partial_y v_x) - f_{xy},$$

$$\dot{\sigma}_{xz} = c_{55}(\partial_x v_z + \partial_z v_x) - f_{xz},$$

$$\dot{\sigma}_{yz} = c_{44}(\partial_y v_z + \partial_z v_y) - f_{yz},$$

The differential equations can be written in matrix form as

$$\dot{\mathbf{v}} + \mathbf{s} = \mathbf{M} \cdot \mathbf{v}, \tag{8}$$

where

$$\mathbf{v} = [v_x, v_y, v_z, \sigma_{xx}, \sigma_{yy}, \sigma_{zz}, \sigma_{xy}, \sigma_{xz}, \sigma_{yz}, T, \psi]^\top \tag{9}$$

is the unknown array vector,

$$\mathbf{s} = [f_x/\rho, f_y/\rho, f_z/\rho, f_{xx}, f_{yy}, f_{zz}, f_{xy}, f_{xz}, f_{yz}, 0, q']^\top \tag{10}$$

is the source vector, and  $\mathbf{M}$  is the propagation matrix containing the spatial derivatives and material properties, where  $q' = (C\tau)^{-1}q$ .

The spatial derivatives are calculated with the Fourier method by using the fast Fourier transform (FFT) (see a brief introduction in the next subsection). We present a time-integration method based on the Crank-Nicolson scheme in Appendix A.

### 3.1 The Fourier Method

In particular, the Fourier pseudospectral method is the central part of the numerical algorithm, since the numerical spatial dispersion must be avoided in view of the physical dispersion caused by the attenuation of the wavefield. This spatial approximation is infinitely accurate for band-limited periodic functions with cutoff spatial wavenumbers which are smaller than the cutoff wavenumbers of the mesh (Carcione [5]).

Let us consider the  $x$  coordinate. A continuous function  $u(x)$  (the wavefield) is approximated by a truncated series

$$u_N(x_j) = \sum_{r=0}^{N-1} \tilde{u}_r \exp(ik_r x_j) = \sum_{r=0}^{N-1} \tilde{u}_r \exp(2\pi i r j / N), \tag{11}$$

where  $\tilde{u}_r$  are spectral coefficients,  $N$  is the number of grid points,

$$x_j = j dx \quad \text{and} \quad k_r = \frac{2\pi r}{N dx}, \quad r = 0, \dots, N - 1, \tag{12}$$

are the collocation (grid) points and wavenumbers, respectively, with  $dx$  the grid spacing and  $i = \sqrt{-1}$ . The spectral (expansion) coefficients are chosen such that the approximate solution  $u_N$  coincides with the solution  $u(x)$  at the collocation points. The Fourier method is appropriate for problems with periodic boundary conditions – for example, a wave which exits the grid on one side, and reenters it on the opposite side.

The sequence  $u(x_j)$  is the inverse discrete Fourier transform of

$$\tilde{u}_r = \frac{1}{N} \sum_{j=0}^{N-1} u(x_j) \exp(-2\pi i r j / N) \quad r = 0, \dots, N - 1. \tag{13}$$

**Table 1** Medium properties

density, $\rho$	3162 m/s
$C_{11}, C_{12}, C_{13}$	10, 2, 1.5
$C_{22}, C_{23}, C_{33}$	9, 1, 8
$C_{44}, C_{55}, C_{66}$	3, 2, 1
$v_{11} = \sqrt{c_{11}/\rho}$	3162 m/s
specific heat, $C$	117 kg/(m s <sup>2</sup> °K)
thermal expansion, $\alpha_1 = \alpha_2 = \alpha_3$	$0.33 \times 10^{-5}$ °K <sup>-1</sup>
absolute temperature, $T_0$	300 °K,
relaxation time, $\tau = \gamma/(Cv_{11}^2)$	854,701 s

The computation of an spatial derivative of order  $L$  by the Fourier method conveniently reduces to a set of multiplications of the different coefficients  $\tilde{u}_r$ , with factors  $(ik_r)^L$ , since

$$\partial_x^L u_N(x_j) = \sum_{r=0}^{N-1} (ik_r)^L \tilde{u}_r \exp(ik_r x_j). \quad (14)$$

The spectral coefficients  $\tilde{u}_r$  are computed by the FFT. The steps of the calculation of the first-order fractional partial derivative are as follows:

$$u(x_j) \rightarrow \text{FFT} \rightarrow \tilde{u}_r \rightarrow (ik_r)^L \tilde{u}_r \rightarrow \text{FFT}^{-1} \rightarrow \partial_x^L u(x_j). \quad (15)$$

$L = 1$  is employed in the algorithm of Appendix A.

## 4 Physics and Simulations

We consider the properties listed in Table 1, where  $C_{IJ} = c_{IJ}/\rho$  is given in (km/s)<sup>2</sup> (e.g.,  $c_{11} = 2.65C_{11}$  in GPa). These values yield

$$\beta_1 = 118,057, \quad \beta_2 = 104,940, \quad \beta_3 = 91,822 \quad (16)$$

in kg/(m s<sup>2</sup> °K). Moreover, let us consider anisotropy of the thermal conductivity, i.e.,

$$\gamma_1 = 10^{15} \text{ m kg/(s}^3 \text{ °K)}, \quad \gamma_2 = \gamma_1/2, \quad \gamma_3 = 2\gamma_1/3. \quad (17)$$

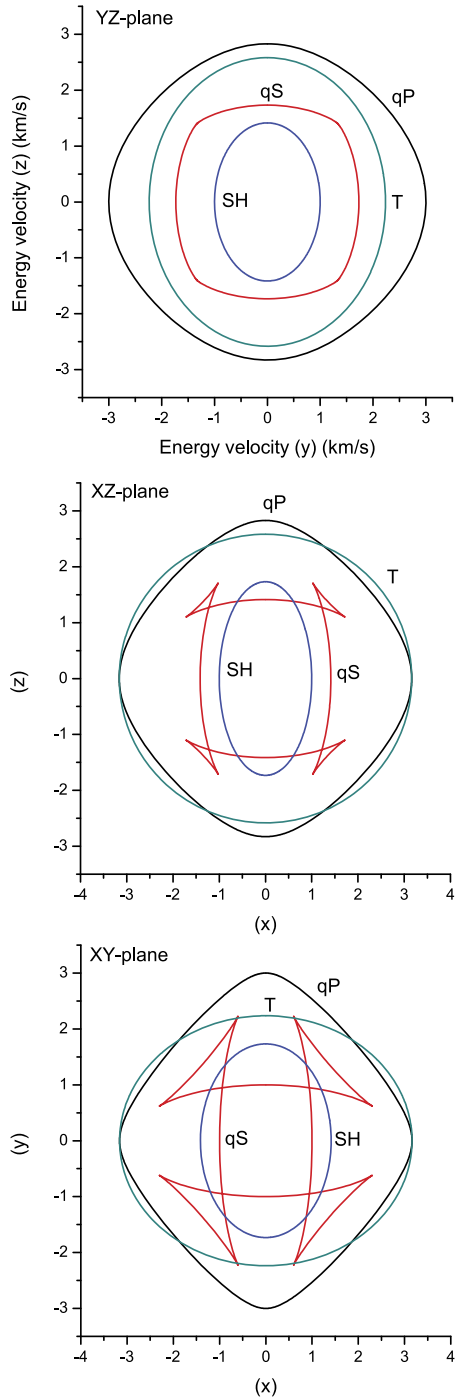
Initially, we consider a positive thermal expansion. A plane-wave analysis is performed in Appendix B, where the wavefronts of the four modes are obtained in the uncoupled case, i.e., the heat equation is not coupled to the elasticity equations ( $\beta_i = 0$ ) and the dispersion equation for the coupled case is established. Figure 1 shows the energy velocities of the various wave modes. We observe the anisotropic behavior of all the waves, including the thermal one.

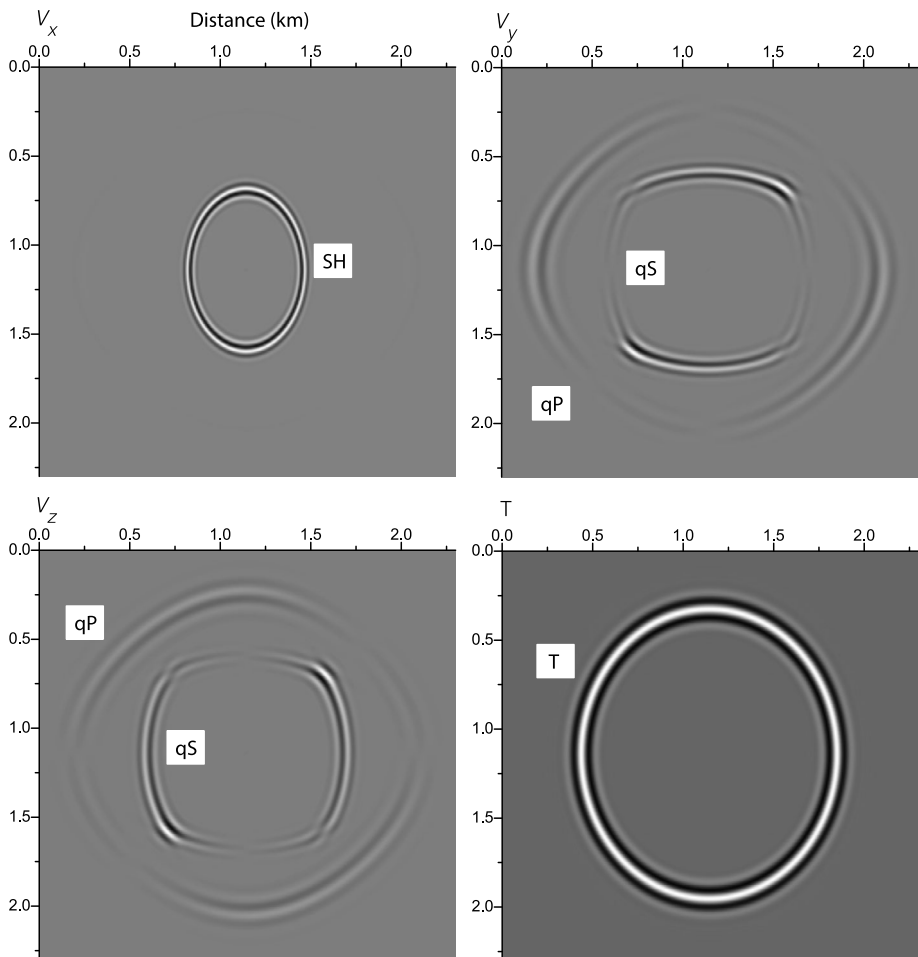
Next, we obtain snapshots of the wavefield, where we consider a  $231 \times 231$  mesh and grid spacing  $dx = dy = dz = 10$  m. The source is located at the center of the mesh and has the time history

$$h(t) = \cos[2\pi(t - t_0)f_0] \exp[-2(t - t_0)^2 f_0^2], \quad (18)$$

where  $f_0$  is the central frequency and  $t_0 = 3/(2f_0)$  is a delay time.

**Fig. 1** Energy velocities of the various wave modes in the uncoupled case. The heat equation is not coupled to the elasticity equations ( $\beta_i = 0$ )





### YZ-plane

**Fig. 2** Snapshots of the wavefield in the uncoupled case (YZ-plane). The source is  $f_x = f_y = f_z = q = 1$ . The heat equation is not coupled to the elasticity equations ( $\beta_i = 0$ )

We assume  $f_0 = 25$  Hz and run the simulations with  $dt = 0.5$  ms. Figures 2, 3 and 4 show snapshots of the particle-velocity components in the YZ, XZ and XY symmetry planes at 250 ms in the uncoupled case. The source is composite (heat and directional elastic), i.e.,  $q = 1$ ,  $f_x = f_y = f_z = 1$ . We can clearly see the qP and qS waves in the snapshots and the pure SH wave as expected in the YZ-plane ( $v_x$ -component), XZ-plane ( $v_y$ -component) and XY-plane ( $v_z$ -component), being this wave and antiplane mode. The T wave is anisotropic, in agreement with the curves in Fig. 1. In relative terms, if we consider the amplitudes of the  $v_x$  snapshot in the XZ-planes and  $T$  snapshot in the XY-plane to have a maximum amplitude of 1, the relative amplitudes in absolute value,  $\max(v_x, v_y, v_z, T)$  are: YZ-plane: (0.5, 0.9, 0.8, 1), XZ-plane: (1, 0.5, 0.7, 1), XY-plane: (0.94, 0.75, 0.56, 1). For the choice of  $\tau$  given above, the T-wave velocity is close to the P-wave velocity. As we shall see, elastic-heat coupling reduces the T-wave velocity.

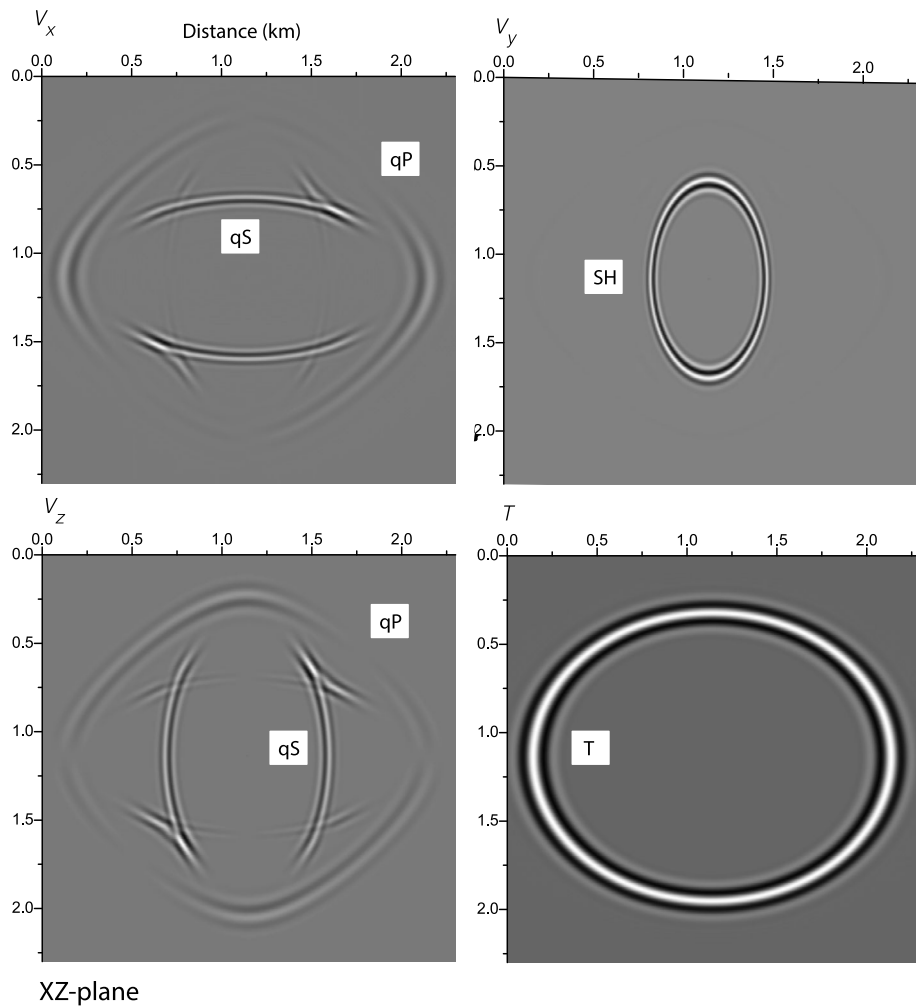
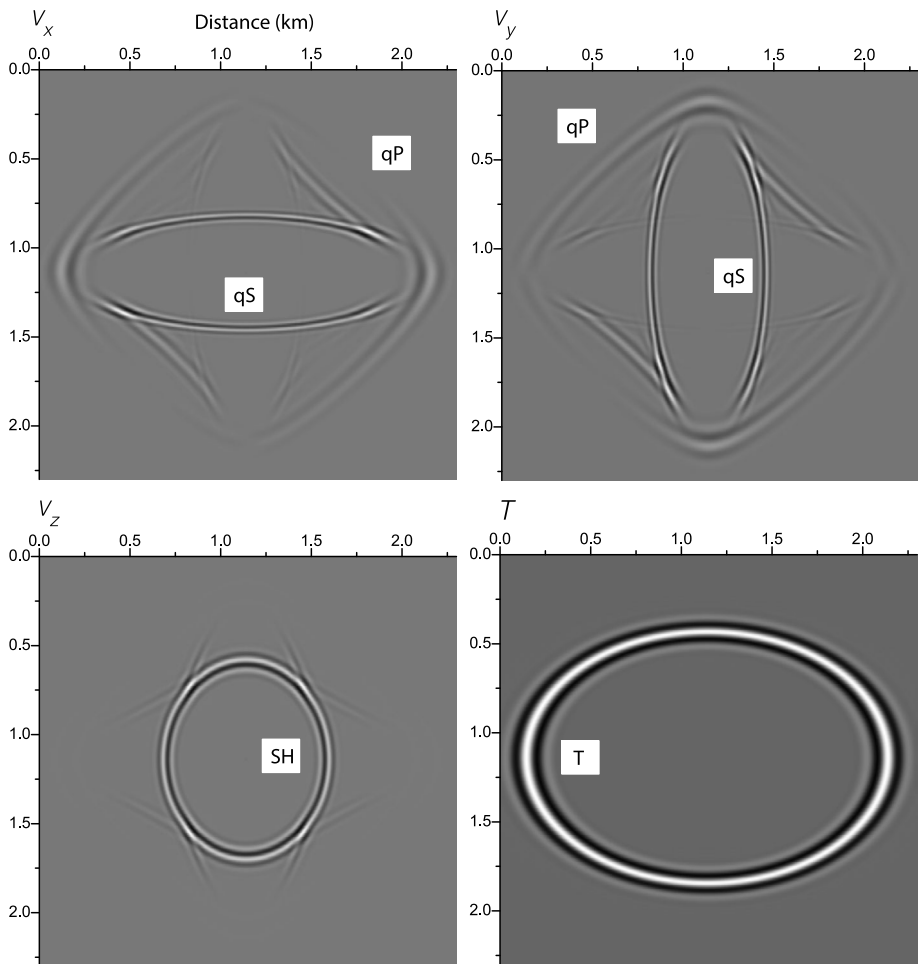


**Fig. 3** Snapshots of the wavefield in the uncoupled case ( $XZ$ -plane). The source is  $f_x = f_y = f_z = q = 1$ . The heat equation is not coupled to the elasticity equations ( $\beta_i = 0$ )

Let us now consider the coupled case and only a heat source, i.e.,  $q = 1$ . Figure 5 shows the snapshots in all the symmetry planes, with the first, second, third and fourth rows corresponding to  $v_x$ ,  $v_y$ ,  $v_z$  and  $T$ , respectively. The heat source induces elastic motion and the coupling conversion from elastic motion to heat as can be seen in the  $T$  snapshots. The presence of qS waves is due to the coupling between the qP and qS motion. The heat source generates qP waves which in turn generate qS energy. The qS waves in this case are superposed to the T wave, since the velocity of the T waves is close to the S-wave velocity when there is elastic-heat coupling for this particular choice of  $\tau$ . As can be seen, the antiplane fields have zero amplitude (computer noise), because this shear mode is not coupled to the qP mode and heat equation (see diagonal snapshots in Fig. 5). This holds in symmetry planes and homogeneous media. The maximum  $T$  amplitude is 0.3 that of the uncoupled case, indicating that 2/3 of the heat energy has been transformed to elastic energy.

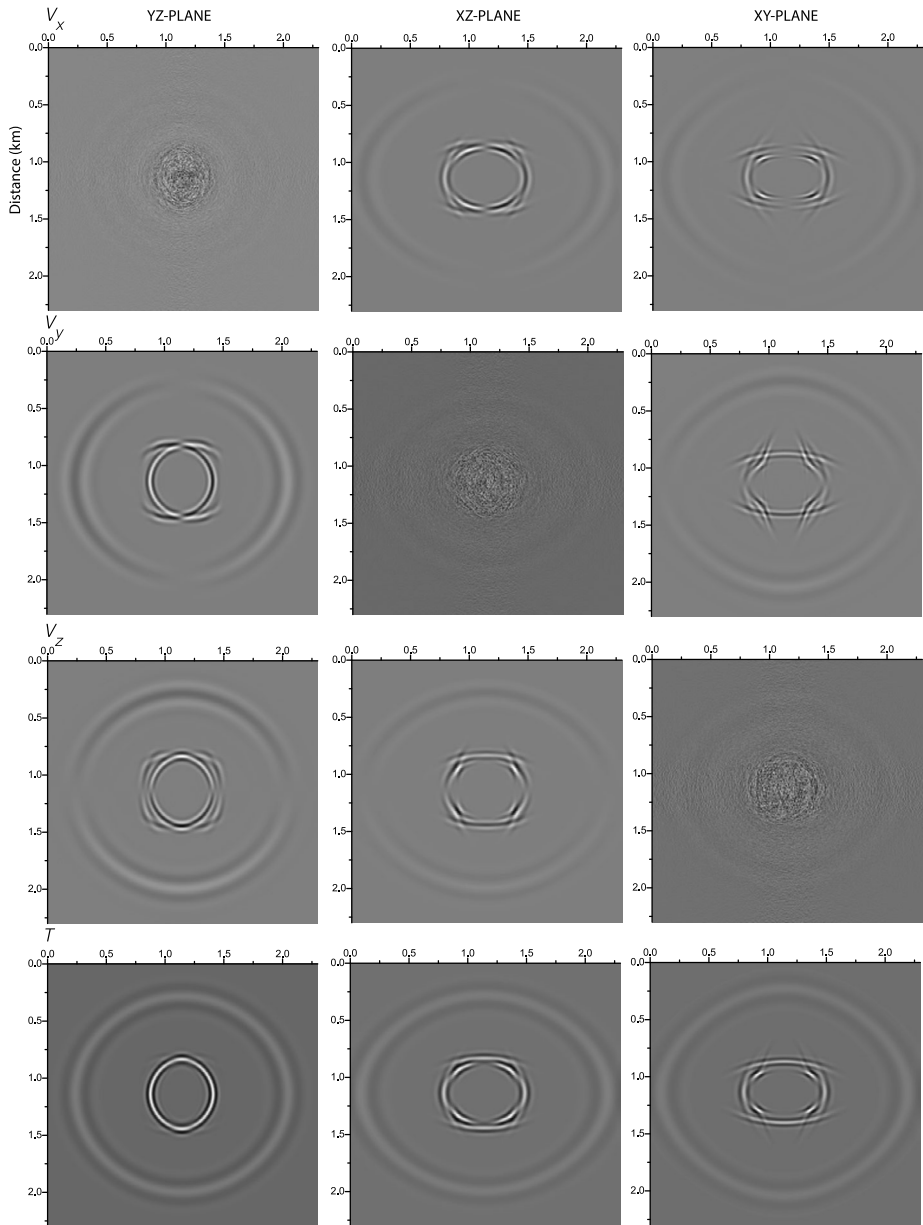


### XY-plane

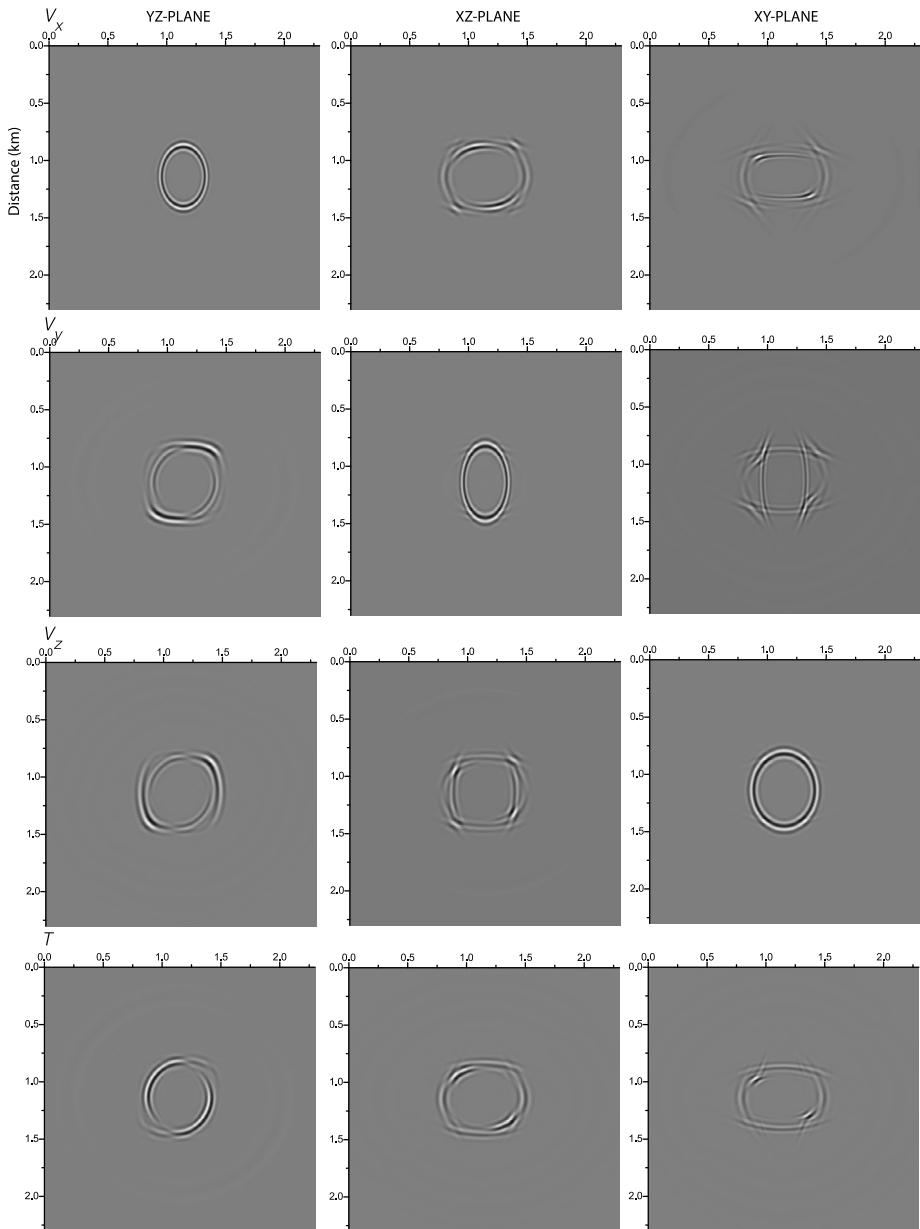
**Fig. 4** Snapshots of the wavefield in the uncoupled case (XY-plane). The source is  $f_x = f_y = f_z = q = 1$ . The heat equation is not coupled to the elasticity equations ( $\beta_i = 0$ )

Figure 6 shows snapshots in the coupled case for a source  $f_x = f_y = f_z = 1$ , i.e., only an elastic source. This source generates qP and qS waves, and T waves due to the elastic/heat coupling (see lower panel). On the other hand, Fig. 7 displays snapshots of  $v_z$  and  $T$  in the YZ-plane and coupled case. The source is  $f_{xx} = f_{yy} = f_{zz} = 1$ , i.e., a dilatational source. The wavelike and diffusive cases correspond to  $\gamma_1 = 10^{15}$  and  $\gamma_1 = 10.5$  (in  $\text{m kg}/(\text{s}^3 \text{ }^\circ\text{K})$ ), respectively. This source would generate P and T waves and part of qS waves due to the qP-qS coupling caused by anisotropy. In the diffusive case, the T wave energy remains at the source location (it disappears as a wave).

Let us now consider the wavelike case and replace  $\tau$  by  $9\tau$ . According to equation (B.8) this choice implies a lower velocity in the uncoupled case (three times lower) and even lower in the coupled case, so that the T and S wavefronts are separated. Taking equation (B.8) as



**Fig. 5** Snapshots of the wavefield in the coupled case. The source is  $q = 1$ , i.e., only a heat source. Since the  $T$  and  $qS$  waves have a similar velocity, the fields are superposed (inner events). In relative terms, if we consider the amplitude of the  $T$  snapshot in the  $XY$ -plane to have a maximum amplitude of 1, the amplitudes in absolute,  $\max(v_x, v_y, v_z, T)$  are:  $YZ$ -plane: (0, 0.05, 0.044, 0.55),  $XZ$ -plane: (0.13, 0, 0.1, 0.86),  $XY$ -plane: (0.16, 0.1, 0.1, 1). The maximum  $T$  amplitude is 0.3 that of the uncoupled case, indicating that 2/3 of the heat energy has been transformed to elastic energy



**Fig. 6** Snapshots of the wavefield in the coupled case. The source is  $f_x = f_y = f_z = 1$ , i.e., only an elastic source. Since the  $T$  and  $qS$  waves have a similar velocity, the fields are superposed (inner events). In relative terms, if we consider the amplitude of the  $T$  snapshot in the  $XY$ -plane to have a maximum amplitude of 1, the amplitudes in absolute,  $\max(v_x, v_y, v_z, T)$  are:  $YZ$ -plane: (0.007, 0.007, 0.007, 0.3),  $XZ$ -plane: (0.01, 0.005, 0.01, 0.8),  $XY$ -plane: (0.018, 0.013, 0.004, 1). The maximum  $T$  amplitude is  $2 \times 10^5$  that of the uncoupled case

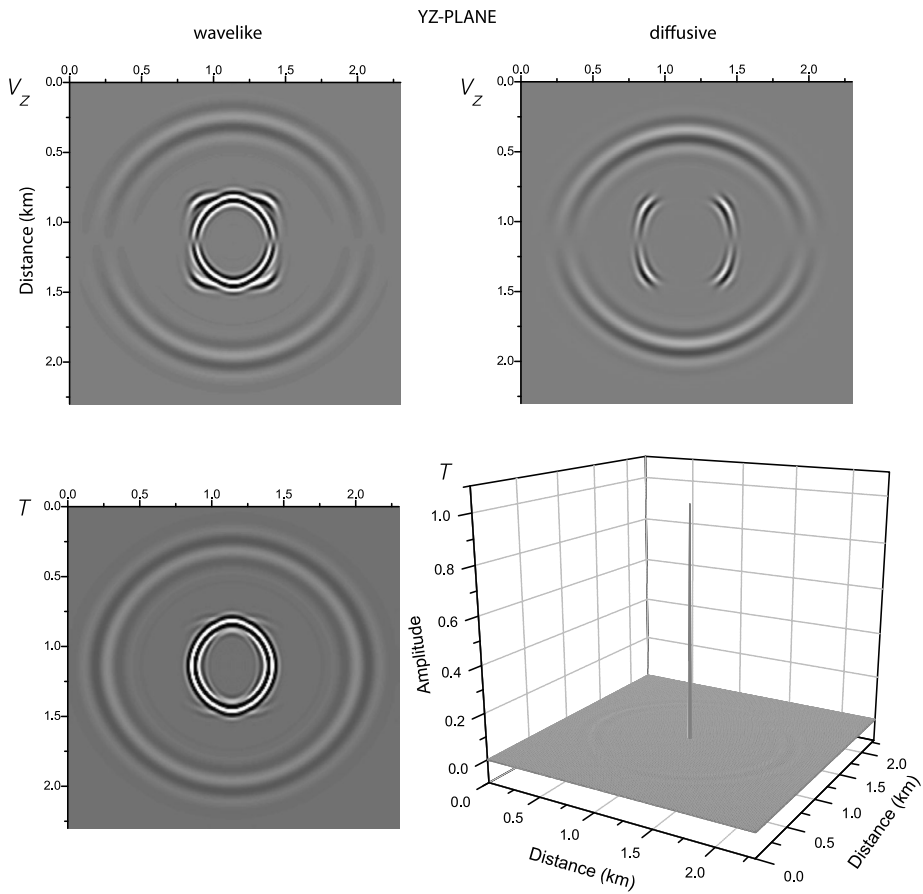


**Fig. 7** Snapshots of  $v_z$  and  $T$  in the YZ-plane and coupled case. The source is  $f_{xx} = f_{yy} = f_{zz} = 1$ , i.e., a dilatational source. The wavelike and diffusive cases correspond to  $\gamma_1 = 10^{15}$  and  $\gamma_1 = 10.5$  (in  $\text{m kg}/(\text{s}^3 \text{ }^\circ\text{K})$ ), respectively

an approximation of the T-wave velocity, we obtain  $c = 745 \text{ m/s}$ , which is the lower one. According to the sampling theorem, the mesh supports frequencies up to  $c/(2 dx) = 37 \text{ Hz}$  ( $dx = 10 \text{ m}$ ,) to avoid spatial aliasing. Hence, we consider a central frequency  $f_0 = 18 \text{ Hz}$ . Figure 8 shows the  $v_x$  and  $T$  wavefields corresponding to the XZ-plane (a), compared to those of Fig. 5 (b), where the source is of heat type only. Figure 9 presents similar results (a) for a source  $f_x = f_y = f_z = 1$ , compared to those of Fig. 6 (b). In both figures, the T wave is stronger and travels with a lower velocity, as expected.

Finally, we consider an inhomogeneous case, where a flat interface perpendicular to the XZ-plane separates an isotropic medium (upper half space) and an anisotropic medium (lower half space). The example is the same of Fig. 5, with the isotropic medium defined by  $C_{22} = C_{33} = C_{11}$ ,  $C_{12} = C_{13} = C_{23} = C_{11} - 2C_{44}$  and  $C_{55} = C_{66} = C_{44}$ . Figure 10 shows a snapshot of the temperature field in the XZ=plane (compare the corresponding snapshot of the lower panel in Fig. 5). As can be observed, the field above the interface has isotropic characteristics.

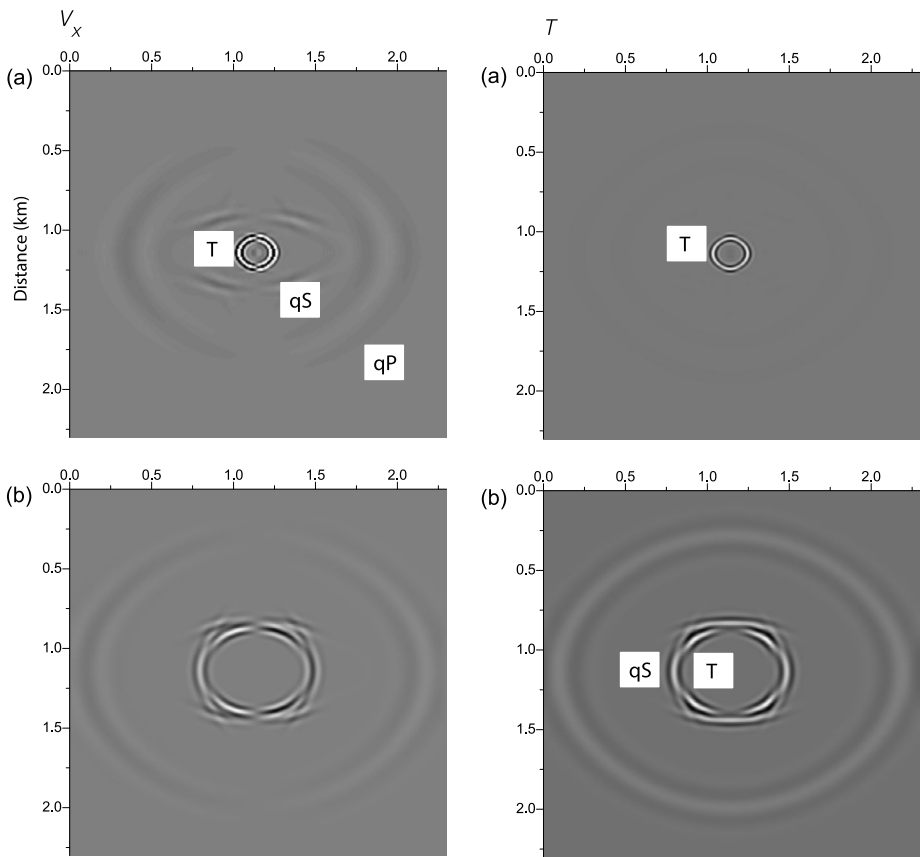


**Fig. 8** Snapshots of the wavefield in the coupled case ( $XZ$ -plane). The source is  $q = 1$ , i.e., only a heat source. The relaxation time  $\tau$  in (a) is nine times higher than of the simulation shown in (b) (see Fig. 5). In this case, the T wave has a much lower velocity than that of the qS wave and the two wavefronts are clearly separated

In simulations with a negative thermal expansion (not shown) the kinematics is not affected. This can easily be seen in isotropic media where the adiabatic velocity of the P wave depends on the thermal expansion coefficient to the power of two (see Carcione [5]; Eq. 7.843 and Fig. 7.30). Moreover, simulations show that the amplitudes are similar to the case of a positive thermal expansion with the same absolute value.

## 5 Conclusions

We have proposed a numerical algorithm to solve the differential equations of anisotropic thermoelasticity, i.e., coupling elasticity with thermal effects. The modeling is a direct-grid method that allows us to handle spatially inhomogeneous media. It is based on the Fourier method to compute the spatial derivatives and a Crank-Nicolson scheme for the time stepping.

A heat source induces elastic motion. The presence of shear waves is due to the coupling between the P and S motion in anisotropic media. In symmetry planes and homogeneous

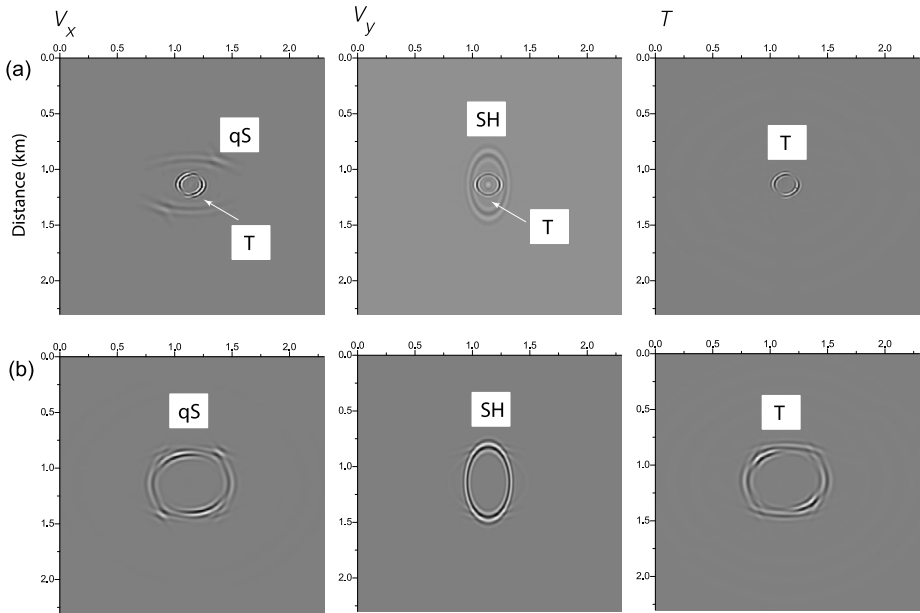
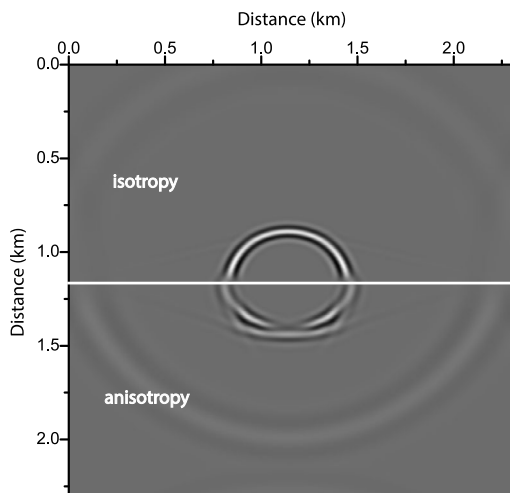


**Fig. 9** Snapshots of the wavefield in the coupled case ( $XZ$ -plane). The source is  $f_x = f_y = f_z = 1$ , i.e., only an elastic source. The relaxation time  $\tau$  in (a) is nine times higher than that of the simulation shown in (b) (see Fig. 6). In this case, the T wave has a much lower velocity than that of the qS wave and the two wavefronts are clearly separated

**Fig. 10** Snapshots of the temperature wavefield in the coupled case ( $XZ$ -plane), where the upper half space is isotropic (refer to Fig. 5, where the whole medium is anisotropic)



media, antiplane fields have zero amplitude, because this shear mode is not coupled to the P mode and heat equation. An elastic source generates P and S waves, and T (thermal) waves due to the elastic/heat coupling. In the diffusive case, the T wave energy remains at the source location (disappears as a wave). Increasing the relaxation time implies a lower T-wave velocity in the uncoupled case (three times lower) and even lower in the coupled

case. In simulations with a negative thermal expansion the kinematics is not affected and the amplitude is hardly affected, at least for the specific example considered here.

### Appendix A: Crank-Nicolson Explicit Scheme

The explicit Crank-Nicolson explicit scheme has been introduced by Carcione and Quiroga-Goode [7] to solve the equations of poroelasticity, and subsequently used to solve the thermoelasticity equations in the isotropic case (Carcione et al. [9]). The scheme, adapted to the anisotropic case, is

$$\begin{aligned}
 D^{1/2}v_x &= \rho^{-1}(\partial_x\sigma_{xx}^n + \partial_y\sigma_{xy}^n + \partial_z\sigma_{xz}^n - f_x^n) = \Pi_x^n, \\
 D^{1/2}v_y &= \rho^{-1}(\partial_x\sigma_{xy}^n + \partial_y\sigma_{yy}^n + \partial_z\sigma_{yz}^n - f_y^n) = \Pi_y^n, \\
 D^{1/2}v_z &= \rho^{-1}(\partial_x\sigma_{xz}^n + \partial_y\sigma_{yz}^n + \partial_z\sigma_{zz}^n - f_z^n) = \Pi_z^n, \\
 \epsilon_1 &= \partial_x A^{1/2}v_x, \quad \epsilon_2 = \partial_y A^{1/2}v_y, \quad \epsilon_3 = \partial_z A^{1/2}v_z, \\
 \dot{\epsilon}_1 &= \partial_x \Pi_x^n, \quad \dot{\epsilon}_2 = \partial_y \Pi_y^n, \quad \dot{\epsilon}_3 = \partial_z \Pi_z^n, \\
 \Delta_\gamma T^n &= C(A^{1/2}\psi + \tau D^{1/2}\psi) \\
 &\quad + T_0[\beta_1(\epsilon_1 + \tau\dot{\epsilon}_1) + \beta_2(\epsilon_2 + \tau\dot{\epsilon}_2) + \beta_3(\epsilon_3 + \tau\dot{\epsilon}_3)] + q^n, \\
 T^{n+1} &= T^n + dt \psi^{n+1/2}, \\
 D^1\sigma_{xx} &= c_{11}\epsilon_1 + c_{12}\epsilon_2 + c_{13}\epsilon_3 - \beta_1 A^{1/2}\psi - f_{xx}^n, \\
 D^1\sigma_{yy} &= c_{12}\epsilon_1 + c_{22}\epsilon_2 + c_{23}\epsilon_3 - \beta_2 A^{1/2}\psi - f_{yy}^n, \\
 D^1\sigma_{zz} &= c_{13}\epsilon_1 + c_{23}\epsilon_2 + c_{33}\epsilon_3 - \beta_3 A^{1/2}\psi - f_{zz}^n, \\
 D^1\sigma_{xy} &= c_{66}(\partial_x A^{1/2}v_y + \partial_y A^{1/2}v_x) - f_{xy}^n, \\
 D^1\sigma_{xz} &= c_{55}(\partial_x A^{1/2}v_z + \partial_z A^{1/2}v_x) - f_{xz}^n, \\
 D^1\sigma_{yz} &= c_{44}(\partial_y A^{1/2}v_z + \partial_z A^{1/2}v_y) - f_{yz}^n,
 \end{aligned} \tag{A.1}$$

where

$$D^j \phi = \frac{\phi^{n+j} - \phi^{n-j}}{2jdt}, \quad \text{and} \quad A^j \phi = \frac{\phi^{n+j} + \phi^{n-j}}{2}, \tag{A.2}$$

are the central differences and mean value operators, based on a Crank-Nicolson (staggered) implicit scheme (Jain [17], p. 269) for the particle velocities. In this three-level scheme,  $(v_x, v_z, \psi)$  at time  $(n + 1/2)dt$  and stresses and temperature at time  $(n + 1)dt$  are computed explicitly from  $(v_x, v_z, \psi)$  at time  $(n - 1/2)dt$  and stresses and temperature at time  $(n - 1)dt$  and  $ndt$ , respectively.

The sixth equation yields

$$\begin{aligned}
 &(dt + 2\tau)\psi^{n+1/2} \\
 &= \frac{2dt}{C}[\Delta_\gamma T^n - T_0[\beta_1(\epsilon_1 + \tau\dot{\epsilon}_1) + \beta_2(\epsilon_2 + \tau\dot{\epsilon}_2) + \beta_3(\epsilon_3 + \tau\dot{\epsilon}_3)] - q^n] \\
 &\quad - (dt - 2\tau)\psi^{n-1/2}.
 \end{aligned} \tag{A.3}$$

An example of stability analysis has been performed in Carcione and Quiroga-Goode [7], i.e., a Von Neumann stability analysis based on the eigenvalues of the amplification matrix (Jain [17], p. 418). The algorithm has first-order accuracy but possesses the stability properties of implicit algorithms and the solution can be obtained explicitly.

## Appendix B: Plane-Wave Analysis

A general solution representing inhomogeneous viscoelastic plane waves is of the form

$$[\cdot] \exp[i(\omega t - \mathbf{k} \cdot \mathbf{x})], \quad (\text{B.1})$$

where  $[\cdot]$  is a constant complex vector,  $\omega$  is the angular frequency and

$$\mathbf{k} = \kappa - i\boldsymbol{\alpha} = (\kappa - i\boldsymbol{\alpha})\hat{\mathbf{k}} \equiv k\hat{\mathbf{k}}, \quad (\text{B.2})$$

is the complex wavenumber vector, with  $\kappa$  and  $\boldsymbol{\alpha}$  the real wavevector and attenuation vector, respectively. The second equality holds for homogeneous waves, where  $k = \kappa - i\boldsymbol{\alpha}$  is the complex wavenumber and  $\hat{\mathbf{k}} = (l_1, l_2, l_3)$  defines the propagation (and attenuation) direction, where  $l_i$  are the directions cosines.

In thermoelasticity,

$$(\mathbf{v}, T) \propto \exp[ik(v_c t - (l_1 x + l_2 y + l_3 z))], \quad (\text{B.3})$$

where

$$v_c = \frac{\omega}{k} \quad (\text{B.4})$$

is the complex velocity.

### B.1 Uncoupled Case

In the uncoupled case,  $\beta_i = 0$  and the elasticity equations correspond to a lossless orthorhombic medium, whose properties are well known (e.g., Carcione [5], Chap. 1). Substituting the plane wave (B.3) into the heat equation (5), we obtain, for homogeneous waves, the following complex velocity for the T wave:

$$v_c = \sqrt{\frac{\omega G}{i\eta C}}, \quad (\text{B.5})$$

where

$$G = \gamma_1 l_1^2 + \gamma_2 l_2^2 + \gamma_3 l_3^2 \quad (\text{B.6})$$

and

$$\eta = 1 + i\omega\tau. \quad (\text{B.7})$$

The velocity ranges from 0 at low frequencies to

$$v = \sqrt{\frac{G}{\tau C}} \quad (\text{B.8})$$

at high (infinite) frequencies, the latter being the phase velocity related of the wavefront.

The actual wavefront velocity is given by the envelope velocity, whose components and absolute value are (Carcione [5], Sect. 1.4.3), i.e.

$$v_{env})_i = \frac{\partial v}{\partial l_i} = \frac{\gamma_i l_i}{v\tau C}, \quad i = 1, \dots, 3. \tag{B.9}$$

and

$$v_{env} = \frac{1}{v\tau C} \sqrt{\gamma_1^2 l_1^2 + \gamma_2^2 l_2^2 + \gamma_3^2 l_3^2}, \tag{B.10}$$

respectively. In the isotropic case, we have  $v_{env} = \gamma / (v\tau C) = v$ .

A more strict approach to obtain the velocity of the wavefront associated with each Fourier component is based on an energy balance that gives the energy velocity (e.g., Banerjee and Pao [2]). This and the envelope velocity are the same in the lossless case and high and low frequency limits (see Carcione [5], Sect. 1.4.3 and 4.6.3), and it is the case that for certain diffusion equations both velocities coincide (Carcione [5], Eq. 7.813).

The phase velocity vector is

$$\mathbf{v}_p = \left(\frac{\omega}{\kappa}\right) \hat{\mathbf{k}} = \left[\text{Re}\left(\frac{1}{v_c}\right)\right]^{-1} \hat{\mathbf{k}} \tag{B.11}$$

and the attenuation vector is

$$\boldsymbol{\alpha} = -\omega \text{Im}\left(\frac{1}{v_c}\right) \hat{\mathbf{k}} \tag{B.12}$$

(Carcione [5]).

### B.2 Coupled Case

Substituting the plane wave (B.3) into the heat equation (5), we obtain for homogeneous waves

$$T = -\nu(\beta_1 \epsilon_1 + \beta_2 \epsilon_2 + \beta_3 \epsilon_3), \tag{B.13}$$

where the  $\epsilon$  are strains here, and

$$\nu = \frac{\eta T_0}{(\gamma_1 l_1^2 + \gamma_2 l_2^2 + \gamma_3 l_3^2)k^2 + i\omega C\eta}. \tag{B.14}$$

Substituting equation (B.13) into (2) gives

$$\begin{aligned} \sigma_{xx} &= p_{11}\epsilon_1 + p_{12}\epsilon_2 + p_{13}\epsilon_3 \\ \sigma_{yy} &= p_{12}\epsilon_1 + p_{22}\epsilon_2 + p_{23}\epsilon_3 \\ \sigma_{zz} &= p_{13}\epsilon_1 + p_{23}\epsilon_2 + p_{33}\epsilon_3 \\ \sigma_{xy} &= 2p_{66}\epsilon_{xy}, \\ \sigma_{xz} &= 2p_{55}\epsilon_{xz}, \\ \sigma_{yz} &= 2p_{44}\epsilon_{yz}, \end{aligned} \tag{B.15}$$

where

$$p_{IJ} = c_{IJ} + i\omega\nu\beta_I\beta_J, \quad I = 1, 2, 3, \quad p_{II} = c_{II}, \quad I = 4, 5, 6. \tag{B.16}$$

These  $p_{IJ} = p_{IJ}(l_i, k, \omega)$  depend on the direction cosines and wavenumber  $k$ , because  $\nu = \nu(l_i, k, \omega)$  and  $k$  is the solution of the dispersion equation (see below). In the isothermal anisotropic-viscoelastic case, we have  $p_{IJ} = p_{IJ}(\omega)$ .

Equation (B.15) can be re-written in matrix form as

$$\boldsymbol{\sigma} = \mathbf{P} \cdot \mathbf{e} = (\mathbf{C} + i\omega\nu\mathbf{B}) \cdot \mathbf{e}, \tag{B.17}$$

where

$$\boldsymbol{\sigma} = (\sigma_{xx}, \sigma_{yy}, \sigma_{zz}, \sigma_{yz}, \sigma_{xz}, \sigma_{xy})^\top, \tag{B.18}$$

$$\mathbf{e} = (\epsilon_{xx}, \epsilon_{yy}, \epsilon_{zz}, 2\epsilon_{yz}, 2\epsilon_{xz}, 2\epsilon_{xy})^\top, \tag{B.19}$$

$$\mathbf{C} = \begin{pmatrix} c_{11} & c_{12} & c_{13} & 0 & 0 & 0 \\ c_{12} & c_{22} & c_{23} & 0 & 0 & 0 \\ c_{13} & c_{23} & c_{33} & 0 & 0 & 0 \\ 0 & 0 & 0 & c_{44} & 0 & 0 \\ 0 & 0 & 0 & 0 & c_{55} & 0 \\ 0 & 0 & 0 & 0 & 0 & c_{66} \end{pmatrix} \tag{B.20}$$

and

$$\mathbf{B} = \begin{pmatrix} \beta_1^2 & \beta_1\beta_2 & \beta_1\beta_3 & 0 & 0 & 0 \\ \beta_1\beta_2 & \beta_2^2 & \beta_2\beta_3 & 0 & 0 & 0 \\ \beta_1\beta_3 & \beta_2\beta_3 & \beta_3^2 & 0 & 0 & 0 \\ 0 & 0 & 0 & 0 & 0 & 0 \\ 0 & 0 & 0 & 0 & 0 & 0 \\ 0 & 0 & 0 & 0 & 0 & 0 \end{pmatrix}, \tag{B.21}$$

Matrix  $\mathbf{P} = \mathbf{C} + i\omega\nu\mathbf{B}$  is symmetric, as in the isothermal case.

Let us consider the time-space domain. In the absence of external forces, the equation of motion and strain-displacement relation are in the Voigt notation,

$$\mathbf{e} = \nabla^\top \cdot \mathbf{u}, \quad (e_I = \nabla_{Ij}u_j), \quad j = 1, 2, 3 \quad I = 1, \dots, 6 \tag{B.22}$$

and

$$\nabla \cdot \boldsymbol{\sigma} = \rho \ddot{\mathbf{u}} \tag{B.23}$$

(Carcione [5], Eqs. 1.26 and 1.28), respectively, where

$$\mathbf{u} = (u_1, u_2, u_3) \tag{B.24}$$

is the displacement vector, and

$$\nabla = \begin{pmatrix} \partial_1 & 0 & 0 & 0 & \partial_3 & \partial_2 \\ 0 & \partial_2 & 0 & \partial_3 & 0 & \partial_1 \\ 0 & 0 & \partial_3 & \partial_2 & \partial_1 & 0 \end{pmatrix}. \tag{B.25}$$

is an spatial-derivative operator.

For the plane waves (B.1), the operator (B.25) takes the form

$$\nabla \rightarrow -i\mathbf{K}, \tag{B.26}$$

where

$$\mathbf{K} = \begin{pmatrix} k_1 & 0 & 0 & 0 & k_3 & k_2 \\ 0 & k_2 & 0 & k_3 & 0 & k_1 \\ 0 & 0 & k_3 & k_2 & k_1 & 0 \end{pmatrix} = k \begin{pmatrix} l_1 & 0 & 0 & 0 & l_3 & l_2 \\ 0 & l_2 & 0 & l_3 & 0 & l_1 \\ 0 & 0 & l_3 & l_2 & l_1 & 0 \end{pmatrix} \equiv k\mathbf{L}, \tag{B.27}$$

with  $k_1, k_2$  and  $k_3$  being the components of the complex wavevector  $\mathbf{k}$ .

Using equations (B.26) and (B.27)), and combining equations (B.17)), (B.22) and (B.23), we obtain

$$k^2 \mathbf{\Gamma}(k) \cdot \mathbf{u} = \rho \omega^2 \mathbf{u}, \tag{B.28}$$

where

$$\mathbf{\Gamma} = \mathbf{L} \cdot \mathbf{P} \cdot \mathbf{L}^\top \tag{B.29}$$

is the symmetric Kelvin-Christoffel matrix,

Unlike the isothermal case,  $\mathbf{\Gamma} = \mathbf{\Gamma}(v_c)$ , i.e., it depends on the complex velocity (B.4). Equation (B.28) yields

$$\mathbf{A} \cdot \mathbf{u} = 0, \quad \text{with } \mathbf{A} = \mathbf{\Gamma}(v_c) - \rho v_c^2. \tag{B.30}$$

This is a nonlinear eigenvalue problem (Effenberg [13]; Voss [34]). A non-zero solution for  $\mathbf{u}$  requires:

$$\det \mathbf{A} = 0. \tag{B.31}$$

In the orthorhombic case,

$$\begin{aligned} \Gamma_{11} &= p_{11}l_1^2 + p_{66}l_2^2 + p_{55}l_3^2, \\ \Gamma_{22} &= p_{66}l_1^2 + p_{22}l_2^2 + p_{44}l_3^2, \\ \Gamma_{33} &= p_{55}l_1^2 + p_{44}l_2^2 + p_{33}l_3^2, \\ \Gamma_{12} &= (p_{12} + p_{66})l_1l_2, \\ \Gamma_{13} &= (p_{13} + p_{55})l_3l_1, \\ \Gamma_{23} &= (p_{44} + p_{23})l_2l_3 \end{aligned} \tag{B.32}$$

(Carcione [5]).

An alternative approach to solve the coupled case is the following. For the plane wave (B.3), the stress strain relation (2) and momentum equation (B.23) can be written in matrix form as

$$\boldsymbol{\sigma} = \mathbf{C} \cdot \mathbf{e} - \beta T = -ik\mathbf{C} \cdot \mathbf{L}^\top \cdot \mathbf{u} - \beta T \tag{B.33}$$

and

$$ik\mathbf{L} \cdot \boldsymbol{\sigma} = \rho \omega^2 \mathbf{u}, \tag{B.34}$$

respectively, where

$$\boldsymbol{\beta} = (\beta_1, \beta_2, \beta_3, 0, 0, 0)^\top. \quad (\text{B.35})$$

Combining the two equations, we obtain

$$\omega(\boldsymbol{\Gamma} - \rho v_c^2 \mathbf{I}_3) \cdot \mathbf{u} + i v_c \mathbf{L} \cdot \boldsymbol{\beta} T = 0, \quad (\text{B.36})$$

where here

$$\boldsymbol{\Gamma} = \mathbf{L} \cdot \mathbf{C} \cdot \mathbf{L}^\top \quad (\text{B.37})$$

is the isothermal Kelvin-Christoffel matrix.

On the other hand, the heat equation becomes

$$\omega v_c \eta T_0 \boldsymbol{\beta}^\top \cdot \mathbf{L}^\top \cdot \mathbf{u} + (\omega G + i C \eta v_c^2) T = 0. \quad (\text{B.38})$$

Equations (B.36) and (B.38) can be re-written in matrix form as

$$\begin{pmatrix} \omega(\boldsymbol{\Gamma} - \rho v_c^2 \mathbf{I}_3) & i v_c \mathbf{L} \cdot \boldsymbol{\beta} \\ \omega v_c \eta T_0 \boldsymbol{\beta}^\top \cdot \mathbf{L}^\top & (\omega G + i C \eta v_c^2) \end{pmatrix} \cdot \begin{pmatrix} \mathbf{u} \\ T \end{pmatrix} = 0. \quad (\text{B.39})$$

Equations (B.36) and (B.38) provide a non-trivial solution for  $\mathbf{u}$  and  $T$  if the determinant of their coefficients vanishes,

$$\det [(\omega G + i C \eta v_c^2)(\boldsymbol{\Gamma} - \rho v_c^2 \mathbf{I}_3) - i \eta T_0 v_c^2 (\mathbf{L} \cdot \boldsymbol{\beta}) \cdot (\boldsymbol{\beta}^\top \cdot \mathbf{L}^\top)] = 0, \quad (\text{B.40})$$

which gives the complex velocity  $v_c$  as solution.

In the uncoupled case,  $\boldsymbol{\beta} = 0$  and we have the isothermal case and a pure heat equation with complex velocity (B.5).

The solution of the coupled case will be treated in a separate paper.

**Author contributions** JMC and JB wrote the main manuscript and EW, ANQ and MA contributed to the modeling. All authors reviewed the manuscript.

## Declarations

**Competing interests** The authors declare no competing interests.

## References

1. Armstrong, B.H.: Models for thermoelastic in heterogeneous solids attenuation of waves. *Geophysics* **49**, 1032–1040 (1984)
2. Banerjee, D.K., Pao, Y.-H.: Thermoelastic waves in anisotropic solids. *J. Acoust. Soc. Am.* **56**(5), 1444–1454 (1974)
3. Biot, M.A.: Thermoelasticity and irreversible thermodynamics. *J. Appl. Phys.* **27**, 240–253 (1956)
4. Boschi, E.: A thermoviscoelastic model of the earthquake source mechanism. *J. Geophys. Res.* **78**, 7733–7737 (1973)
5. Carcione, J.M.: *Wave Fields in Real Media. Theory and Numerical Simulation of Wave Propagation in Anisotropic, Anelastic, Porous and Electromagnetic Media*, 4th edition, extended and revised. Elsevier, Amsterdam (2022)
6. Carcione, J.M., Gei, D., Santos, J.E., Fu, L.-Y., Ba, J.: Canonical analytical solutions of wave-induced thermoelastic attenuation. *Geophys. J. Int.* **221**, 835–842 (2020)

7. Carcione, J.M., Quiroga-Goode, G.: Some aspects of the physics and numerical modeling of Biot compressional waves. *J. Comput. Acoust.* **3**, 261–280 (1995)
8. Carcione, J.M., Wang, E., Cavallini, F., Ba, J., Fu, L.-Y.: Physics and simulation of wave propagation in linear thermo-poroelastic media. *J. Geophys. Res.* (2019). <https://doi.org/10.1029/2019JB017851>
9. Carcione, J.M., Wang, Z.-W., Ling, W., Salusti, E., Ba, J., Fu, L.-Y.: Simulation of wave propagation in linear thermoelastic media. *Geophysics* **84**, T1–T11 (2019)
10. Cattaneo, C.: Sur une forme de l'équation de la chaleur éliminant paradoxe d'une propagation instantanée. *C. R. Acad. Sci.* **247**, 431–433 (1958)
11. Deresiewicz, H.: Plane waves in a thermoelastic solid. *J. Acoust. Soc. Am.* **29**, 204–209 (1957)
12. Dhaliwal, R.S., Sherief, H.H.: Generalized thermoelasticity for anisotropic media. *Q. Appl. Math.* **38**, 1–8 (1980)
13. Effenberg, C.: Robust solution methods for nonlinear eigenvalue problems. PhD thesis, EPFL, Lausanne (2013)
14. Green, A.E., Lindsay, K.A.: Thermoelasticity. *J. Elast.* **2**(1), 1–7 (1972)
15. Gurevich, B., Carcione, J.M.: Attenuation and dispersion in fluid-saturated porous rocks: mechanisms and models. SEG publication nr. 26 (2022)
16. Jacquey, A.B., Cacace, M., Guido Blöcher, G., Scheck-Wenderoth, M.: Numerical investigation of thermoelastic effects on fault slip tendency during injection and production of geothermal fluids. *Energy Proc.* **76**, 311–320 (2015)
17. Jain, M.K.: Numerical Solutions of Partial Differential Equations. Wiley, New York (1984)
18. Karunarathne, A., Parajuli, P., Priyadarshan, G., Bhattacharya, S., Rao, R., Wei, P.-C., Chen, Y.-Y., Gladson, J.R., Rao, A.M.: Anisotropic elasticity drives negative thermal expansion in monocrystalline SnSe. *Phys. Rev. B* **103**, 054108 (2021)
19. Kolyano, Y.M., Shter, E.I.: Application of the variational principle to the solution of generalised coupled problems in thermoelasticity of inhomogeneous media. *J. Eng. Phys.* **42**, 84–88 (1982)
20. Lord, H., Shulman, Y.: A generalized dynamical theory of thermoelasticity. *J. Mech. Phys. Solids* **15**, 299–309 (1967)
21. Romao, C.P., Donegan, S.P., Zwanzigerade, J.W., White, M.A.: Relationships between elastic anisotropy and thermal expansion in A2Mo3O12 materials. *Phys. Chem. Chem. Phys.* **18**, 30652 (2016)
22. Rudgers, A.J.: Analysis of thermoacoustic wave propagation in elastic media. *J. Acoust. Soc. Am.* **88**(2), 1078–1094 (1990)
23. Savage, J.: Thermoelastic attenuation of elastic waves by cracks. *J. Geophys. Res.* **71**, 3929–3938 (1966)
24. Sellitto, A., Cimmelli, V.A., Jou, D.: Nonlinear propagation of coupled first- and second-sound waves in thermoelastic solids. *J. Elast.* **138**, 93–109 (2020). <https://doi.org/10.1007/s10659-019-09733-z>
25. Sharma, M.D.: Wave propagation in anisotropic generalized thermoelastic media. *J. Therm. Stresses* **29**(7), 629–642 (2006)
26. Sharma, J.N., Singh, H.: Generalized thermoelastic waves in anisotropic media. *J. Acoust. Soc. Am.* **85**(4), 1407–1413 (1989)
27. Singh, B.: Wave propagation in an anisotropic generalized thermoelastic solid. *Indian J. Pure Appl. Math.* **34**(10), 1479–1486 (2003)
28. Tokuoka, T.: Thermo-acoustical waves in linear thermo-elastic materials. *J. Eng. Math.* **7**, 115–122 (1973)
29. Treitel, S.: On the attenuation of small-amplitude plane stress waves in a thermoelastic solid. *J. Geophys. Res.* **64**, 661–665 (1959)
30. Vernotte, P.: Théorie continue et théorie moléculaire des phénomènes thermocinétiques. *C. R. Acad. Sci.* **227**, 43–44 (1948)
31. Verma, K.L.: Thermoelastic vibrations of a transversely isotropic plate with thermal relaxations. *Int. J. Solids Struct.* **38**, 8529–8546 (2001)
32. Verma, K.L.: On the propagation of waves in layered anisotropic media in generalized thermoelasticity. *Int. J. Eng. Sci.* **40**(18), 2077–2096 (2002)
33. Verma, K.L.: Thermoelastic slowness surfaces in anisotropic media with thermal relaxation. *Lat. Am. J. Solids Struct.* **11**, 2227–2240 (2014)
34. Voss, H.: Nonlinear eigenvalue problems. In: *Handbook of Linear Algebra*, 2nd edn. CRC Press, Boca Raton (2014). <https://doi.org/10.1201/b16113-70>. Chapter: 60
35. Wang, E., Carcione, J.M., Cavallini, F., Botelho, M.A.B., Ba, J.: Generalized thermo-poroelasticity equations and wave simulation. *Surv. Geophys.* **42**, 133–157 (2021)
36. Wang, Z.-W., Fu, L.-Y., Carcione, J.M., Hou, W., Wei, J.: Analytical solution of thermoelastic attenuation in fine layering for random variations of the Grüneisen ratio. *J. Therm. Stresses* (2022). <https://doi.org/10.1080/01495739.2022.2074930>
37. Zener, C.: Internal friction in solids. II. General theory of thermoelastic internal friction. *Phys. Rev.* **53**, 90–99 (1938)

**Publisher's Note** Springer Nature remains neutral with regard to jurisdictional claims in published maps and institutional affiliations.

Springer Nature or its licensor (e.g. a society or other partner) holds exclusive rights to this article under a publishing agreement with the author(s) or other rightsholder(s); author self-archiving of the accepted manuscript version of this article is solely governed by the terms of such publishing agreement and applicable law.